Few-body Systems manuscript No.
(will be inserted by the editor)

E. Garrido · A.S. Jensen · D.V. Fedorov

Techniques to treat the continuum applied to electromagnetic transitions in ^{8}Be

Received: date / Accepted: date

Abstract Bremsstrahlung emission in collisions between charged nuclei is equivalent to nuclear gamma decay between continuum states. The way the continuum spectrum can be treated is not unique, and efficiency and accuracy of cross section calculations depend on the chosen method. In this work we describe, relate, and compare three different methods in practical calculations of inelastic cross sections, that is, by (i) treating the initial and final states as pure continuum states on the real energy axis, (ii) discretizing the continuum states on the real energy axis with a box boundary condition, and (iii) complex rotation of the hamiltonian (complex scaling method). The electric quadrupole transitions, $2^+ \to 0^+$ and $4^+ \to 2^+$, in $\alpha + \alpha$ scattering are taken as an illustration.

Keywords First keyword · Second keyword · More

1 Introduction

The emission of bremsstrahlung in a collision between two charged particles constitutes an important background effect in Coulomb deexcitation processes. In a classical picture, this phenomenon is understood as the energy radiated due to the deceleration of a charged particle when deflected by another charged particle. The radiated energy is just the kinetic energy lost in the deceleration process. In a quantum mechanical picture, the process can be seen as the γ-emission due to the decay of a two-body system from some two-body continuum state into another continuum state of lower energy. A detailed derivation of the cross section for this kind of processes can be found in [1].

The fact that these transitions involve continuum structures, both in the initial and final states, introduce technical as well as conceptual difficulties in the calculations. First, the treatment of the continuum spectrum itself, which can be handled in different ways, but in numerical studies almost necessarily by some kind of discretization. Second, the unavoidable matrix elements between the continuum states involved in the calculation are diverging and thus not well defined without some regularization prescription. These two problems, how to treat the continuum and how to obtain converged results, are possible sources of uncertainty that deserves detailed investigations.

Different methods were previously used to compute the bremsstrahlung cross sections for various combinations of nuclei. In [2] $\alpha - \alpha$ collisions were investigated in connection with the resonant electric

E. Garrido
Instituto de Estructura de la Materia, IEM-CSIC, Serrano 123, E-28006 Madrid, Spain
E-mail: e.garrido@csic.es

A.S. Jensen
Department of Physics and Astronomy, Aarhus University, DK-8000 Aarhus C, Denmark

D.V. Fedorov
Department of Physics and Astronomy, Aarhus University, DK-8000 Aarhus C, Denmark

quadrupole capture into the unbound ground state of ^{8}Be. The bremsstrahlung cross section was obtained without any discretization of the continuum spectrum. The two-body states are then pure continuum structures, which are orthogonal to each other in a continuum sense, through a Dirac delta.

Another possibility is for instance employed in [3], where the bremsstrahlung radiation during α-decay was computed in a time dependent picture for heavy nuclei. In this case the continuum states were discretized and treated on the same footing as the discrete part of the spectrum describing the bound states. The orthogonality condition is now given by a Kronecker delta. In both these two procedures the energy is a real number, which means that the resonances (if any) are not isolated as particular continuum states, and their effect on the cross section is diluted into the continuum spectrum (discretized or not).

In [4] the Coulomb breakup reaction of ^{11}Be was analyzed by use of the complex scaling method. This method [5] rotates the usual coordinates into the complex plane ($x \rightarrow x\exp(i\theta)$), and permits an easy separation between resonances and ordinary continuum states. The resonances, defined as poles of the $\mathcal{S}$-matrix, appear as discrete solutions clearly separated from the (rotated) continuum background, provided the rotation angle is sufficiently large. This method provides simultaneously the complex resonance energy with real part and imaginary part equal to minus half the width. The complex energy of the resonance can also be found by extending the energy into the complex plane without any complex rotation of the coordinates. The complex scaling method has the enormous advantage that the resonance wave function falls off exponentially at large distances, exactly as ordinary bound states. This fact permits to circumvent all the technical difficulties arising from the otherwise exponentially divergent resonance wave function. However, the continuum background still contributes and must therefore necessarily be included in calculations of the observable cross sections.

The ^{8}Be nucleus is particularly interesting due to the role it most likely plays in the triple-alpha radiative capture into ^{12}C, which is one of the most important reactions in stellar nucleosyntheses. This nucleus is rather well described as an α+α molecular cluster structure, and therefore equally well treated as a two-body problem. In a recent work [6] the full continuum method was used to investigate the $E2$-transitions in ^{8}Be. In particular, the cross section was found to be insensitive to the α-α interaction used, and it was also shown how a precise definition of the cross section requires a choice of an energy window for the final states in the scattering process.

The existence and energy sequence of the 0^+, 2^+, and 4^+ resonances suggest the interpretation of these states as a rotational band. However, these states are located in the continuum with corresponding decay widths. In other words, continuum properties are an integral part of understanding ^{8}Be. Rotational bands in the continuum present conceptual problems arising from substantial decay widths of these states. This was recently discussed in [7] where the (non-observable) structure dependent electromagnetic transition probabilities approximately were extracted from (observable) cross sections.

Despite the apparent simplicity of ^{8}Be this nucleus is not yet fully understood, because all properties are continuum related, since even the ground state is unbound. Furthermore, ^{8}Be is the only spontaneously fissioning nucleus along the beta-stability line before Uranium. This fission process is complicated due to both dynamics and delicate balancing of various energy terms. On the other hand, the simplicity itself makes ^{8}Be an almost perfect as a test case, since it still is complex enough to maintain essential key features. These should be understood before the properties of more complicated systems can be fully appreciated and exploited.

The purpose of the present work is to describe and compare the three methods mentioned in the paragraphs above. We can then pinpoint when a given method is preferable for computation and interpretation of a given quantity. We can also specifically distinguish between results for the same quantities computed by different methods for the same nucleus. We shall refer to the three methods as the full continuum method, the discretized continuum method, and the complex scaling method. The main aspects of each of them will be given in sections 2, 3, and 4, respectively. The connection between all the three methods will be shown. Each of the three sections contains a subsection where the corresponding method is used to describe the electric quadrupole transitions, $2^+ \rightarrow 0^+$ and $4^+ \rightarrow 2^+$, in ^{8}Be, which are taken as an illustration. We close the paper with the summary and the conclusions.

2 Full continuum method

A detailed derivation of the bremsstrahlung cross section for the collision between two charged particles can be found in Ref. [1]. To be precise, the final result for the differential cross section is given in Eq.(II.3.2) of that reference. A summary of the most relevant expressions can also be found in Ref. [8], where the expressions for the angular integrated cross sections are also given. We first give the expressions for spin-zero bosons which afterwards is applied to collisions between two alpha-particles

2.1 General formulation for spin-zero bosons

The dominating electromagnetic transitions between states of two spin-zero bosons are necessarily of quadrupole character. This applies in particular to the two-alpha system, where Eq.(11) in [8] takes the form:

$$\left.\frac{d\sigma}{dE_\gamma}\right|_{\ell\to\ell'}(E) = \frac{4\pi^2 e^2}{15k^2}\left(\frac{E_\gamma}{\hbar c}\right)^5 (2\ell+1)\left|\langle \ell 0;20|\ell' 0\rangle \int_0^\infty u_\ell(E,r) r^2 u_{\ell'}(E',r) dr\right|^2, \tag{1}$$

where E and E' are the initial and final state energies in the two-body center of mass frame, $E_\gamma = E - E'$ is the energy of the emitted photon, ℓ and ℓ' are the relative angular momenta between the two particles in the initial and final state, e is the unit charge, and $k^2 = 2\mu E/\hbar^2$, where μ is the reduced mass of the two-body system. In Eq.(1) we used a charge of $2e$ for each alpha particle amounting to the factor of $4e^2$.

An important point refers to the radial two-body wave functions u_ℓ and $u_{\ell'}$. They are the solutions of the radial two-body Schrödinger equation:

$$\left[-\frac{\hbar^2}{2\mu}\frac{d^2}{dr^2} + \frac{\hbar^2}{2\mu}\frac{\ell(\ell+1)}{r^2} + V(r) - E\right] u_\ell(E,r) = 0 \tag{2}$$

where $V(r)$ is the two-body interaction. These wave functions behave asymptotically as:

$$u_\ell(E,r) \overset{r\to\infty}{\longrightarrow} C\left[\cos\delta_\ell F_\ell(kr) + \sin\delta_\ell G_\ell(kr)\right], \tag{3}$$

where F_ℓ and G_ℓ are the regular and irregular Coulomb functions, δ_ℓ is the nuclear phase shift, and the asymptotic constant C is determined from the energy normalization condition, which requires that:

$$\int_0^\infty u_\ell(E,r) u_\ell(E',r) dr = \delta(E-E'). \tag{4}$$

This normalization condition implies that the asymptotic constant C has to be:

$$C = \sqrt{\frac{2\mu}{\pi\hbar^2 k}}. \tag{5}$$

A derivation of the value of the asymptotic constant can be found in appendix A. Note that from Eqs.(3) and (5) we have that the units of the radial continuum wave functions u are one over square root of Energy times Length, which is also consistent with the normalization condition (4), and which leads to the correct units of length squared divided by energy for the energy differential cross section in Eq.(1).

The total bremsstrahlung cross section, as a function of the incident energy E, is obtained after integration over the energy of the emitted photon:

$$\sigma(E) = \int \left.\frac{d\sigma}{dE_\gamma}\right|_{\ell\to\ell'}(E)\, dE_\gamma. \tag{6}$$

As stated in Ref.[6], the computed cross sections should be obtained in close analogy to the experimental setup, where only a finite range of final relative energies is measured. This means that the integral in Eq.(6) has to be performed only over this precise energy range. We shall often refer to this range as the final energy window.

A delicate point in the calculation of the cross section refers to the procedure employed to obtain the radial integral in Eq.(1). Due to the fact that the continuum wave functions do not converge towards zero at infinity (see Eq.(3)), the integrand in Eq.(1) actually diverge with distance by oscillating with larger and larger amplitude. Some regularization prescription is required to extract the physically meaningful content. This is possible since the matrix elements physically must be well defined, and mathematically as well corresponding to cancellation of the large-distance contributions. A convenient numerical procedure must then be found and applied.

In this work we shall use the Zel'dovich regularization [9], which introduces the regularization factor $e^{-\eta^2 r^2}$ in the diverging radial integrand. Then the desired correct result is obtained in the limit of zero value for the Zel'dovich parameter η. This removes the unwanted large-distance large-amplitude oscillations and the uniquely defined limiting result is obtained for sufficiently small, but finite, values of η. The smaller the value of η the slower the fall off of the radial integrand, and therefore the larger the upper limit required in the radial integral in Eq.(1). Numerically, this obviously becomes more and more difficult since the large-amplitude oscillations cancel each other and consequently must be very accurately computed. The optimum value of η is therefore as large as possible yet sufficiently small to have reached the limit. A different choice is of course possible for the regularization factor. For instance one could use a higher power in the exponent, which would produce a faster attenuation of the tail of the integrand. However, the use a higher power would reduce the range interval of η-values in which the integral stabilizes at the correct result. The choice made in this work is a sort of compromise between how fast the unwanted tail in the integrand is killed and the difficulty of finding a range of η-values in which the integral reaches the $\eta = 0$ value with sufficient accuracy.

2.2 Full continuum wave functions: $E2$-capture in $\alpha + \alpha$ collisions.

The expressions given in the subsection above provide a summary of the most pertinent formulae for computations of bremsstrahlung cross sections. They are from Refs. [2; 10], where the $2^+ \to 0^+$ and $4^+ \to 2^+$ transitions in ^{8}Be were computed. In [2] the Buck $\alpha-\alpha$ potential given in [11] was used, while in [10] the results obtained with the Buck potential and the Ali-Bodmer potential [12] were compared. The main difference between these potentials is in the treatment of the Pauli principle. The Buck potential generates a nodal structure in the two-body wave functions in accordance with microscopic theories [11]. The immediate consequence is the appearance of two bound 0^+-states and one bound 2^+-state in ^{8}Be (with energies -72.79 MeV, -25.88 MeV, and -22.28 MeV, respectively). These spurious states correspond to Pauli forbidden states. On the other hand the Ali-Bodmer potential contains a short-distance repulsion that prevents the appearance of such forbidden states. Both potentials reproduce equally well the $\ell = 0$, $\ell = 2$, and $\ell = 4$ phase shifts (up to $E \sim 20$ MeV), and therefore the corresponding two-body wave functions have the same asymptotic behavior.

Although in [10] the cross section was found to depend quite a lot on the potential used, in subsequent calculations [13] this dependence was reduced significantly. In fact, in our recent work [6] we have shown that the dependence is actually very small, and the cross sections obtained with the Ali-Bodmer and Buck potentials (and even with the phase equivalent version of the Buck potential) can be hardly distinguished. For this reason in this work any discussion about the dependence on the potential will be omitted, and we will show the results obtained with the Buck potential only. In particular, with this potential the 0^+, 2^+, and 4^+ resonances are found at 0.091 MeV, 2.88 MeV, and 11.78 MeV, respectively, and their corresponding widths are 3.6 eV, 1.24 MeV, and 3.57 MeV. These values agree very well with the experimental values given in [14].

Let us first investigate the dependence of the results on the Zel'dovich parameter η. As mentioned above, this parameter enters in the regularization factor $e^{-\eta^2 r^2}$ used to extract the physics from the wildly oscillating integrand in Eq.(1). In Fig. 1 we show the differential cross section (1) for specific values of the initial and final energies E and E' as a function of η. The solid and dashed curves in the figure correspond to the $2^+ \to 0^+$ transition ($\ell = 2, \ell' = 0$ in Eq.(1)) and the $4^+ \to 2^+$ transition ($\ell = 4, \ell' = 2$ in Eq.(1)), respectively. The chosen values for E and E' are 3.0 MeV and 0.092 MeV for the $2^+ \to 0^+$ transition, and 10.0 MeV and 3.0 MeV for the $4^+ \to 2^+$ transition. As seen in the figure, the cross sections are very stable for sufficiently small values of η. This proves that the $\eta \to 0$ limit is properly reached. Values of η smaller than about 0.02 fm^{-1} then provide the converged value of the cross section in the $\eta \to 0$ limit.

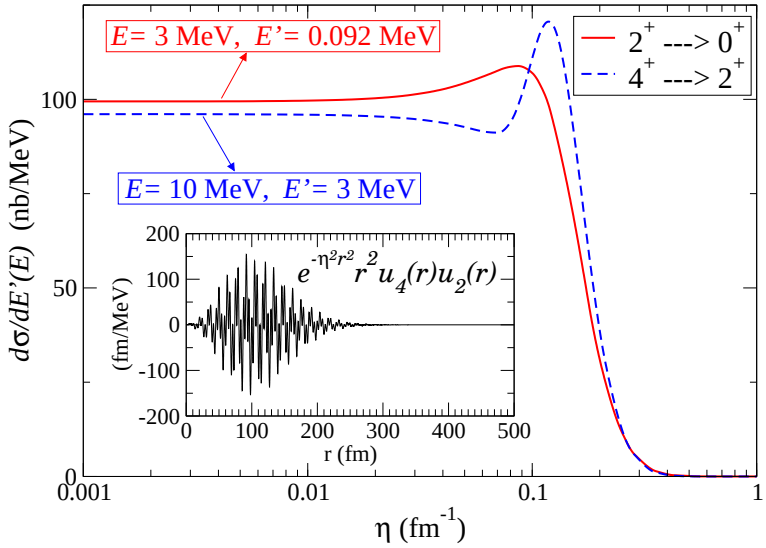

Fig. 1 (Color online) Outer part: Differential cross section (Eq.(1)) for given initial and final energies (E and E') for the $2^+ \to 0^+$ (solid curve) and $4^+ \to 2^+$ (dashed curve) transitions in ^{8}Be as a function of the Zel'dovich parameter η used to regularize the integrand in the radial integral. The values of the initial and final energies are $E = 3.0$ MeV and $E' = 0.092$ MeV for the $2^+ \to 0^+$ transition, and $E = 10.0$ MeV and $E' = 3.0$ MeV for the $4^+ \to 2^+$ transition, respectively. Inner part: Integrand in the radial integral in Eq.(1) corresponding to the differential cross section for the $4^+ \to 2^+$ transition shown in the outer part for $\eta = 0.01$ fm^{-1}.

Furthermore, keeping $\eta \sim 0.01$ fm^{-1} the upper radial limit required in the integral in Eq.(1) stays within reasonable values, such that the integral is not difficult to handle. As an example, we show in the inner part of Fig.1 the integrand corresponding to the $4^+ \to 2^+$ transition shown in the outer part for $\eta = 0.01$ fm^{-1}. As we can see, an upper limit of about 400∼500 fm is enough. In case of using for instance $\eta = 0.001$ fm^{-1} the upper limit moves up til about 5000 fm, and integration of such a highly oscillating function up to that distance becomes a much more delicate task. Of course, the larger the value of η the more the integrand is killed, and eventually, for sufficiently large values of η the computed differential cross section approaches zero. All the results shown later on in this work will be obtained with $\eta = 0.01$ fm^{-1}. We emphasize that the strongly oscillating integrand is a result of the two regularly oscillating continuum wave functions $(u_\ell, u_{\ell'})$. The strong cancellation is a consequence, and the resulting well-defined value of the integral is orders of magnitude smaller than corresponding to the amplitude of the oscillations at the moderate distances, see the inset in Fig.1.

We have then computed the total bremsstrahlung cross section for the $2^+ \to 0^+$ and $4^+ \to 2^+$ transitions according to Eqs.(1) and (6). The 0^+, 2^+, and 4^+ continuum wave functions are computed numerically by solving Eq.(2) for an arbitrarily small grid of energies E and E' ($E_\gamma = E - E' > 0$). The computed wave functions are scaled such that the asymptotic behavior is given by Eqs.(3) and (5). Another important ingredient in the calculation is the final energy window for the integral in Eq.(6). For the $2^+ \to 0^+$ transition it was shown in Ref.[6] that, due to the very small width of the 0^+ resonance in ^{8}Be, a final energy window for the 0^+ states of 0.5 keV around the 0^+ resonance energy is enough to reach convergence for the cross section. This width for the window is far smaller than the best experimental resolution of about 10 keV. For the $4^+ \to 2^+$ transition the cross section is much more sensitive to the size of the final energy window chosen in Ref.[6]. In the present work we shall use the same window as in [10; 13; 15], namely, 2 MeV $< E' <$ 4 MeV, which roughly corresponds to the 2^+-resonance energy ± 1 MeV and also is comparable to its widths of 1.24 MeV.

In Fig. 2 the solid lines show the computed total bremsstrahlung cross section integrated over the corresponding energy windows (Eq.(6)) for the $2^+ \to 0^+$ (Fig.2a) and $4^+ \to 2^+$ (Fig.2b) transitions in ^{8}Be. In both figures the open circles are the results obtained with the Buck potential used in Refs.[2] and [10]. The procedure described in this section is very similar to the one used in these two references, and therefore it is not surprising to find the good agreement between our results and the ones in [2; 10]. However, it is important to keep in mind that when using a different $\alpha - \alpha$ potential (for instance the

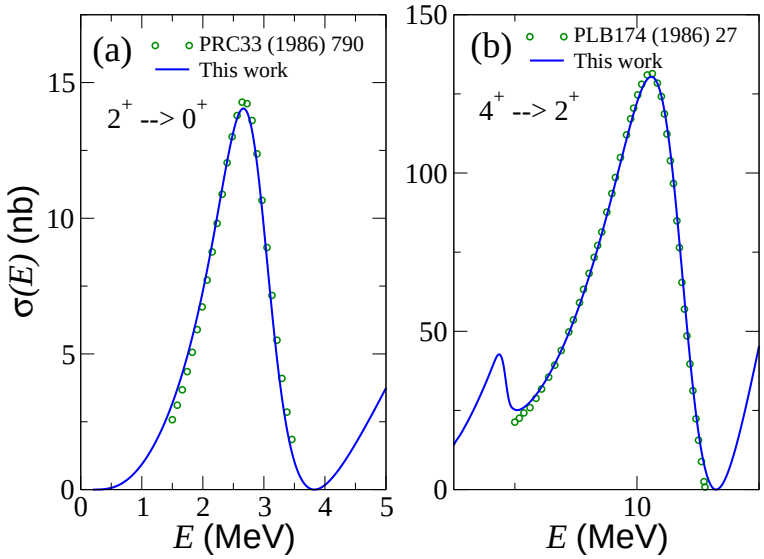

Fig. 2 (Color online) Integrated bremsstrahlung cross section (Eq.(6)) for the (a) $2^+ \to 0^+$ and (b) $4^+ \to 2^+$ transitions in ^{8}Be as a function of the incident energy E. The integral in Eq.(6) has been performed over the final energy windows specified in the text. The open circles in parts (a) and (b) correspond to the cross section obtained with the Buck potential in Refs. [2] and [10], respectively.

Ali-Bodmer potential), we obtain a very similar cross section, while in [10; 13] a big discrepancy was found for the $4^+ \to 2^+$ transitions (see [6] for details). The peak at low energies observed in Fig.2b is due to the known $1/E_\gamma$ dependence of the bremsstrahlung cross section at small photon energies [16]. This is the so called infrared catastrophe. However, as explained in [16], this divergence is not physical. A transition with $E_\gamma = 0$ is nothing but an elastic process. A relativistic treatment of the elastic reaction up to the same order will produce a similar $1/E_\gamma$ divergence in the cross section but with opposite sign that precisely cancels the one obtained in the calculation of the bremsstrahlung cross section. As shown in [6], removal of the soft-photon contributions removes as well the nonphysical peak in the cross section.

3 Discretized continuum method

Instead of using continuum wave functions with the energy normalization in Eq.(4), a quite common procedure is to discretize the continuum spectrum into an orthogonal set of basis functions, and treat them similarly to bound states. One option, rather often used, is to average the continuum states over narrow range of energies. For each of these energy bins a discrete bin wave function is constructed [18; 19]. These wave functions are automatically normalized to 1 provided that the radius of the bin wave function is large enough. In this work we shall employ the much simpler procedure of imposing a box boundary condition. In this way the spectrum is automatically discretized, and each state is then normalized to 1. We first give the general expressions in some details, and then apply to collisions of two alpha-particles.

3.1 General formulation

The connection between the continuum wave functions used in the previous section and the discrete ones can be seen rather easily. To do it, let us assume that we have discretized the continuum spectrum in a box of size L. We then get a family of discrete states $\left\{u_\ell^{(i)}(E_i, r)\right\}$ satisfying that

$$\int_0^L u_\ell^{(i)}(E_i, r) u_\ell^{(j)}(E_j, r) dr = \delta_{ij}. \tag{7}$$

Each state i corresponds to some discrete energy value E_i, and it satisfies the box boundary condition $u_\ell^{(i)}(E_i, L) = 0$. The set of energy values $\{E_i\}$ is then not arbitrary, but dictated by the size of the box. The number of discrete states grows linearly with L, and therefore, the larger L the smaller the energy separation between the discrete states.

Asymptotically each function $u_\ell^{(i)}(E_i, r)$ behaves as $\sim \sin(k_i r + \delta)$, where δ is the phase shift and

$$k_i^2 = 2\mu E_i/\hbar^2. \tag{8}$$

Imposing now that $u_\ell^{(i)}(E_i, L) = 0$, we get that the discrete values of the momentum k_i take the form:

$$k_i \approx i\pi/L; \qquad (i = 1, 2, \cdots), \tag{9}$$

from which, and making use of Eq.(8), it is not difficult to see that the energy separation between two consecutive discrete states is given by:

$$\Delta E = E_i - E_{i-1} = (k_i^2 - k_{i-1}^2)\frac{\hbar^2}{2\mu} \approx \frac{2\pi}{L}\frac{\hbar^2 k_i}{2\mu} = \frac{2\pi}{L}\frac{E_i}{k_i}, \tag{10}$$

where we have assumed that i is large enough such that $(i^2 - (i-1)^2) \approx 2i$. From the expression above it is now evident that the energy distance between two consecutive energies decreases linearly with L.

Let us now use the relation between the Dirac and Kronecker deltas:

$$\delta(E_i - E_j) = \lim_{\Delta E \to 0} \frac{\delta_{ij}}{\Delta E}, \tag{11}$$

where ΔE is the separation between the two energies. From this expression the normalization conditions (7) and (4) can be easily related:

$$\int_0^\infty u_\ell(E_i, r) u_\ell(E_j, r) dr = \lim_{L\to\infty} \int_0^L \frac{u_\ell^{(i)}(E_i, r)}{\sqrt{\Delta E}} \frac{u_\ell^{(j)}(E_j, r)}{\sqrt{\Delta E}} dr, \tag{12}$$

where the wave functions $u_\ell(E, r)$ are continuum functions in the sense of section 2, and where we have used that, as seen in Eq.(10), to impose $\Delta E \to 0$ amounts to imposing $L \to \infty$.

Making use again of Eq.(10), we can relate the pure continuum wave functions and the discrete wave functions. This relation is given by:

$$u_\ell(E_i, r) = \lim_{\Delta E \to 0} \frac{u_\ell^{(i)}(E_i, r)}{\sqrt{\Delta E}} = \lim_{L\to\infty} \sqrt{\frac{L}{2}} \sqrt{\frac{2\mu}{\pi\hbar^2 k_i}} u_\ell^{(i)}(E_i, r). \tag{13}$$

From this expression one can see that while the units of the continuum wave functions u_ℓ are one over square root of Energy times Length, (consistent with (4)), the discrete states $u_\ell^{(i)}$ have units of one over square root of length (consistent with (7)).

Furthermore, taking into account the asymptotic behavior of the continuum wave functions, which is given by Eqs.(3) and (5), it is now evident that the discretized continuum states satisfy:

$$u_\ell^{(i)}(E_i, r) \overset{r\to\infty}{\longrightarrow} \sqrt{\frac{2}{L}} \left[\cos\delta_\ell F_\ell(k_i r) + \sin\delta_\ell G_\ell(k_i r)\right]. \tag{14}$$

Now, in order to compute the bremsstrahlung cross section Eq.(1), the only remaining point is to translate the radial integral in this equation into the discrete continuum spectrum language. To do so, let us first write the square of the radial integral in a more compact way as:

$$\left| \int_0^\infty u_\ell(E, r) r^2 u_{\ell'}(E', r) dr \right|^2 = \langle u_\ell(E, r)| r^2 |u_{\ell'}(E', r)\rangle \langle u_{\ell'}(E', r)| r^2 |u_\ell(E, r)\rangle. \tag{15}$$

Since the discrete continuum states form a complete basis, we can now exploit the completeness relation

$$\mathbb{1} = \sum_i |u_\ell^{(i)}(E_i, r)\rangle \langle u_\ell^{(i)}(E_i, r)|, \tag{16}$$

which of course applies also to the final states with relative orbital angular momentum ℓ'. If we now insert the initial state unity operator in between the u_ℓ functions and r^2, and similarly, the final state unity operator in between the $u_{\ell'}$ functions and r^2, we can then rewrite Eq.(15) as:

$$\left|\int_0^\infty u_\ell(E,r)r^2u_{\ell'}(E',r)dr\right|^2 = \sum_{ij}\langle u_\ell(E,r)|u_\ell^{(i)}(E_i,r)\rangle\langle u_\ell^{(i)}(E_i,r)|r^2|u_{\ell'}^{(j)}(E'_j,r)\rangle\langle u_{\ell'}^{(j)}(E'_j,r)|u_{\ell'}(E',r)\rangle$$
$$\times\sum_{i'j'}\langle u_{\ell'}(E',r)|u_{\ell'}^{(j')}(E'_{j'},r)\rangle\langle u_{\ell'}^{(j')}(E'_{j'},r)|r^2|u_\ell^{(i')}(E_{i'},r)\rangle\langle u_\ell^{(i')}(E_{i'},r)|u_\ell(E,r)\rangle, \quad (17)$$

where the energies with and without primes refer, respectively, to energies in the initial and final states.

Since Eq.(13) can also be written as:

$$u_\ell^{(i)}(E_i,r) = \lim_{\Delta E\to 0}\sqrt{\Delta E}u_\ell(E_i,r), \quad (18)$$

we then have that

$$\langle u_\ell(E,r)|u_\ell^{(i)}(E_i,r)\rangle = \lim_{\Delta E\to 0}\sqrt{\Delta E}\;\delta(E-E_i), \quad (19)$$

and Eq.(17) becomes:

$$\left|\int_0^\infty u_\ell(E,r)r^2u_{\ell'}(E',r)dr\right|^2 = \lim_{\Delta E\to 0}\sum_{ij}\Delta E\delta(E-E_i)\delta(E'-E'_j)\langle u_\ell^{(i)}(E_i,r)|r^2|u_{\ell'}^{(j)}(E'_j,r)\rangle$$
$$\times\sum_{i'j'}\Delta E\delta(E'-E'_{j'})\delta(E-E_{i'})\langle u_{\ell'}^{(j')}(E'_{j'},r)|r^2|u_\ell^{(i')}(E_{i'},r)\rangle. \quad (20)$$

Finally, from Eq.(11) we have that

$$\lim_{\Delta E\to 0}\Delta E\delta(E-E_i)\delta(E-E_{i'}) = \lim_{\Delta E\to 0}\Delta E\delta(E-E_i)\delta(E_i-E_{i'}) = \delta(E-E_i)\delta_{ii'}, \quad (21)$$

and two of the summations in Eq.(20) can be trivially made, which leads to the final result:

$$\left|\int_0^\infty u_\ell(E,r)r^2u_{\ell'}(E',r)dr\right|^2 = \sum_{ij}\delta(E-E_i)\delta(E'-E'_j)\left|\langle u_\ell^{(i)}(E_i,r)|r^2|u_{\ell'}^{(j)}(E'_j,r)\rangle\right|^2, \quad (22)$$

where

$$\langle u_\ell^{(i)}(E_i,r)|r^2|u_{\ell'}^{(j)}(E'_j,r)\rangle = \int_0^L u_\ell^{(i)}(E_i,r)r^2u_{\ell'}^{(j)}(E'_j,r)dr. \quad (23)$$

Therefore, in the discretized continuum picture, the differential bremsstrahlung cross section is given by Eq.(1), where the square of the radial integral is given by (22). Thanks to the delta functions the integral (6) can be trivially made, and we get for the integrated cross section:

$$\sigma(E) = \frac{4\pi^2e^2}{15k^2}(2\ell+1)\langle\ell 0;20|\ell'0\rangle^2\sum_{i,j}\left(\frac{E_\gamma}{\hbar c}\right)^5\delta(E-E_i)\left|\langle u_\ell^{(i)}(E_i,r)|r^2|u_{\ell'}^{(j)}(E'_j,r)\rangle\right|^2 \quad (24)$$

In practice, the total cross section above is computed by making use of Eq.(11) and replacing the δ-function by $\delta_{E,E_i}/\Delta E$, which by use of Eq.(10), permits finally to write the total cross section Eq.(24) as:

$$\sigma(E_i) = \frac{4\pi^2e^2}{15k_i^2}(2\ell+1)\langle\ell 0;20|\ell'0\rangle^2\frac{L}{2\pi}\frac{k_i}{E_i}\sum_j\left(\frac{E_\gamma}{\hbar c}\right)^5\left|\langle u_\ell^{(i)}(E_i,r)|r^2|u_{\ell'}^{(j)}(E'_j,r)\rangle\right|^2 \quad (25)$$

with $E_\gamma = E_i - E'_j$. Since $E_\gamma > 0$ it is then obvious that the summation in j involves all the continuum final states with energy E'_j smaller than the energy E_i of the initial state.

Also, in the same way that the integration Eq.(6) is restricted to final energies within a chosen final energy window, in Eq.(25) the summation over j is also restricted to those discrete final states whose energy E'_j is contained is that energy window. It is important to note that to reach a sufficient

accuracy in the calculation it is necessary to have a significant amount of discrete final energies within that window. This is because the relation Eq.(11), thoroughly used in the description of the discretized continuum procedure, requires a sufficiently small value of ΔE (or equivalently, a sufficiently large value of the box size L) to be valid. In fact, the summation over j in Eq.(25) is actually taking care in the discretized picture of the integral Eq.(6), and it is reasonable to think that too few terms in this summation can not reproduce properly the value of the integral.

Another issue to note is that, as it has to be, the total cross section Eq.(25) is independent of the size of the box L, of course provided L is sufficiently large. This is because the number of states in the summation over j increases linearly with L, which together with the L factor that explicitly appears in Eq.(25) gives a total L^2-dependence. This L^2-factor cancels with the $1/L^2$ dependence of the square of the matrix element in Eq.(25). This $1/L^2$ dependence is evident from the normalization of the asymptotic wave function Eq.(14).

As a final remark, let us mention that Eq.(24), and therefore also Eq.(25), is consistent with the standard expression for the γ-decay cross section, as given for instance in Eq.(4) of Ref. [20]. The details about this consistency are given in appendix B.

3.2 Discrete continuum states in a box: $E2$-capture in $\alpha + \alpha$ collisions.

As done in the previous section, we shall now compute the $E2$-bremsstrahlung cross sections in $\alpha + \alpha$ collisions using the procedure described above.

As already mentioned, use of Eq.(25) requires a sufficiently small energy separation ΔE between the discrete continuum states, such that the number of terms involved in the summation over j is large enough to reproduce the correct value of the integral Eq.(6). Typically, for a reasonably smooth function, about $20 - 30$ terms can be taken as a lower limit for the number of states to be included in the summation. Therefore, given a final energy window, use of Eq.(10) permits to estimate the size of the box L needed for a reasonable description of the process.

For instance, for the $4^+ \to 2^+$ transition considered in Fig.2b, where the final energy window is $2 \text{ MeV} < E' < 4 \text{ MeV}$, an energy separation between states of about 0.1 MeV would give rise to around 20 discrete states within the window. According to Eq.(10), for two alpha-particles and $E_i = 3$ MeV, we get that in order obtain $\Delta E \sim 0.1$ MeV we need the size of the box to be $L \sim 350$ fm. For the $2^+ \to 0^+$ reaction (Fig.2a) the energy window has a width of only 1 keV, which means that the required separation energy between the discrete 0^+ states should be of at most of about 0.1 keV. If we again use Eq.(10) with $E_i = 0.1$ MeV ($\sim 0^+$ resonance energy) we obtain that to get such a small energy separation we would need $L \sim 65000$ fm. This value would be even three orders of magnitude bigger in case of looking for separation energies of the order of 0.1 eV, which would be actually more reasonable, since the width of the 0^+ resonance in ^{8}Be is of just a few eV.

The huge size of the box estimated for the $2^+ \to 0^+$ transition is far beyond our numerical capability, and makes the discretization method completely useless in this particular case. This is due to the fact that the width of the window is orders of magnitude smaller than the energy in the center of the window. Only when these two values are comparable we can say that the use of the discretization method really makes sense. For this reason, in this section we shall consider only the case of the $4^+ \to 2^+$ transition.

As before, the 4^+ and 2^+ wave functions have been obtained by solving Eq.(2) with the Buck α-α potential [11]. They have been computed by imposing a box boundary condition, where normalization automatically is ensured. However, the matrix elements are still strongly oscillating, and the physical meaning has to be extracted as by using the full continuum method as described in Section 2. Again we use the Zel'dovich prescription where each of the oscillating wave functions are multiplied by the Zel'dovich factor, $e^{-\eta^2 r^2/2}$. This changes the normalization to be a function of η and the matrix elements should be correspondingly computed with this η-dependent normalization. In the limit of $\eta \to 0$ the original box-normalization is recovered and the radial integral is obtained precisely as for continuum wave functions. The convergence properties and the range of acceptable parameters are therefore unchanged. In the numerical results we use the value $\eta = 0.01$ fm^{-1} for the Zel'dovich parameter. This implies that the minimum size of the box should be of about $L = 500$ fm, since this value of L guarantees that the integral in Eq.(25) has already converged (see inset of Fig.1). Finally, the corresponding cross section has been computed according to Eq.(25).

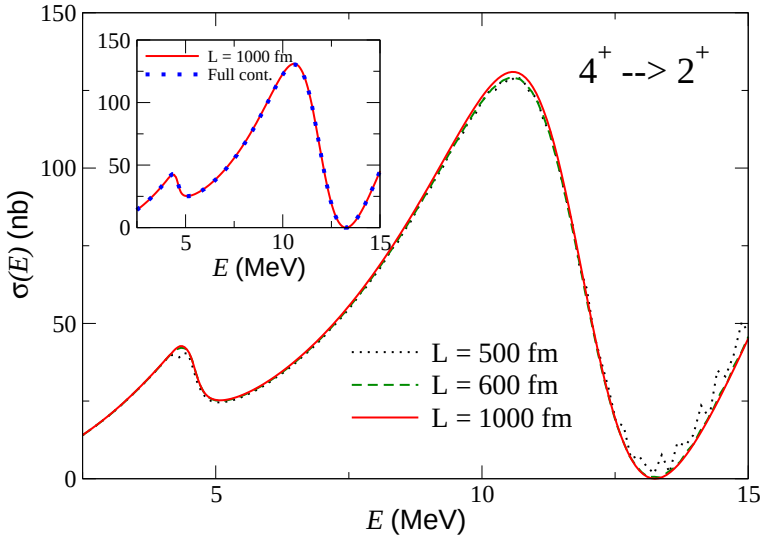

Fig. 3 The same as in Fig. 2b but using continuum states discretized with a box boundary condition. The dotted, dashed, and solid curves have been obtained with a box size of $L = 500$, 600, and 1000 fm, respectively. The inset compares the result obtained with $L = 1000$ fm (solid curve) and the cross section shown in Fig.2b obtained with the full continuum calculation (dotted curve).

To test the dependence on the size of the box, we have performed the calculation for different values of L. In Fig.3 the dotted curve is the cross section obtained with $L = 500$ fm. We can see that, specially for high energies, the curve does not show a smooth behavior. This is due to numerical inaccuracies produced by a still not large enough number of discrete 2^+ states in the final energy window (30 states). In fact, if we reduce L down to 400 fm (only 23 discrete states in the window), the non-smooth behavior is much more pronounced (although not shown in the figure for the sake of clearness). On the other hand, an increase of L up to 600 fm (36 discrete states within the window), permits already to get a smooth cross section, as shown by the dashed curve in the figure. When increasing the value of L, and therefore increasing as well the number of states inside the energy window, a small correction is found for the cross section. This is shown by the solid curve, which has been obtained with $L = 1000$ fm (60 discrete 2^+ states in the energy window). Further increase of L does not produce any visible change when compared to the solid curve in the figure. Finally, in the inset we compare the converged cross section obtained with $L = 1000$ fm (solid curve) and the one shown in Fig.2b, obtained with the full continuum method, and plotted in the inset of Fig.3 by the dotted curve. As we can see the agreement is perfect.

4 Complex Scaling Method

It is well known that when the energy in Eq.(2) is allowed to be complex, bound states and resonances can be identified as poles of the S-matrix in the complex momentum plane. In particular, bound states are located in the positive side of the imaginary axis, and the resonances appear in the fourth quadrant of the plane. The asymptotic behavior Eq.(14) for complex values of the momentum k implies that while the bound states are falling off exponentially at large distances, the resonance wave functions do actually diverge also exponentially.

The numerical difficulties arising from this divergence can however be easily solved by use of the complex scaling method [5; 22]. Its application requires only rotation of the radial coordinate into the complex plane by some arbitrary angle θ ($r \rightarrow re^{i\theta}$). Under this simple transformation, and provided that θ is larger than the argument of the resonance, the complex rotated resonance wave function behaves asymptotically as a bound state, i.e., it falls off exponentially. The same behavior is maintained for bound states. Therefore, after complex scaling, resonances appear formally as "bound states" with complex energy.

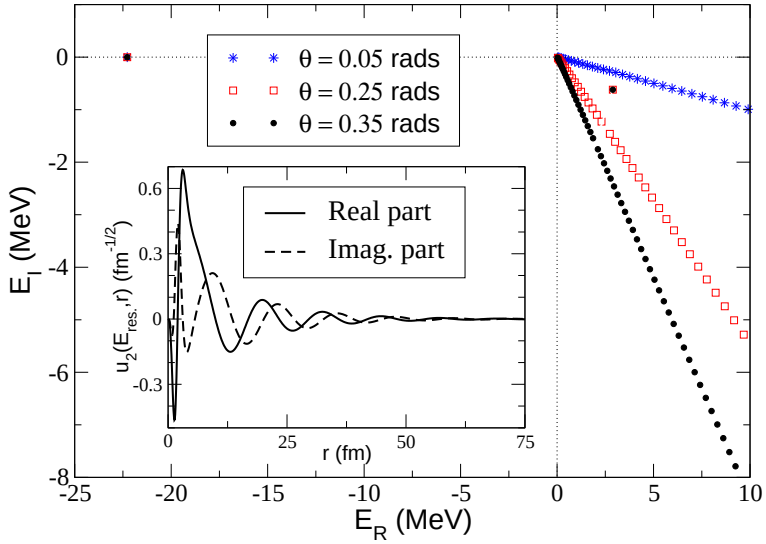

Fig. 4 Outer part: Complex rotated spectrum, in the complex energy plane, of the 2^+ states in ^{8}Be after solving the complex rotated Schrödinger equation (2) with the Buck potential [11], and a box boundary condition. The spectrum is shown for scaling angles $\theta = 0.05$ rads. (stars), $\theta = 0.25$ rads. (squares), and $\theta = 0.35$ rads. (circles). Inner part: The corresponding complex rotated radial wave function (with $\theta = 0.25$ rads.) for to the 2^+ resonance in ^{8}Be.

A complex scaling transformation permits then an easy distinction between continuum states, which are rotated in the complex energy plane by an angle 2θ [5], and resonances, which show up as isolated points whose position is independent of the complex scaling angle used in the calculation. Therefore, this procedure appears as a simple tool allowing separation between different types of contributions: Resonance to resonance, continuum to resonance, resonance to continuum, or continuum to continuum.

In the following, we shall discuss the general properties of the method and its applicability to describe bremsstrahlung processes. Again, we shall apply the method to our test case of two alpha-particles.

4.1 General formulation

As an illustration of the discussion above, we show in the outer part of Fig. 4 the 2^+ spectrum in ^{8}Be after solving the complex rotated Schrödinger equation Eq.(2) with the Buck potential [11], and imposing a box boundary condition to the solutions. The results for three different scaling angles (0.05, 0.25, and 0.35 rads.) are shown by the stars, squares, and circles, respectively. As seen in the figure, the spurious Pauli forbidden bound 2^+ state at about -22.5 MeV is found in all the three calculations. The 2^+ resonance at the complex energy $2.9 - i0.6$ MeV is found as an isolated pole independent of the scaling angle, but only for the two cases where the scaling angle is larger than 0.10 rads, which is the argument of the resonance. The remaining points correspond to the original real energies of continuum 2^+ states rotated in the complex energy plane by an angle 2θ. In the case of $\theta = 0.05$ rads (stars in the figure), the 2^+ resonance is not explicitly found, and its effect on the cross section is then distributed among all the discrete continuum states, as in section 3.

The inner part of the figure shows the complex rotated radial wave function of the 2^+ resonance in ^{8}Be for a complex scaling angle of 0.25 rads. As we can see, for a distance of 75 fm the radial wave function is already pretty small. It is then evident from the figure that after a complex scaling transformation, the integral in Eq.(15) does not diverge anymore, provided that at least one of the states involved in the calculation is a resonance (or a bound state). For transitions between pure continuum states the divergence problem remains, and some regularization (like the Zel'dovich regularization used in this work) would still be necessary.

In order to compute the bremsstrahlung cross section it is then very tempting to make a complex scaling transformation and impose a box boundary condition, which discretizes the spectrum as shown

in Fig. 4. Doing like this, it is also tempting to use the complex scaled version of the method shown in Section 3, which is based on Eqs.(10) and (11), which give the energy separation between the different discrete continuum states and the relation between the Dirac and Kronecker deltas, respectively. In this way the cross section could again be computed as given in Eq.(25), but where the radial wave functions and the r^2 operator have been complex rotated.

However, as shown in Ref.[21], the density of states in the complex rotated continuum does not show the expected behavior. In fact, the simple expression Eq.(9), and therefore also Eq.(10), is found to be valid only in the limit of large rotation angle and large size of the box. This is related to the fact that after complex scaling the resonance states are separated from the other states in the continuum, and therefore one may expect to observe holes in the density of states in the rotating continuum [21] (as actually seen in Fig.4 for the continuum states shown by the squares and the circles, which correspond to complex scaling angles such that the resonance is taken out from the continuum spectrum). In other words, the fact that resonances are isolated in the complex energy plane precludes the use of Eq.(10) in order to transform Eq.(24) into Eq.(25).

The alternative is the method described in [4; 23], where the complex scaling method is used to investigate the transition from the continuum into a bound state. The starting point is the particularization of the transition strength given in appendix B, Eq.(40), where the continuum spectra is assumed to be discretized, to the case of a transition into a bound state. This particularization reads:

$$\frac{d\mathcal{B}^{(\lambda)}}{dE}(J' \to J) = \sum_i \langle \Phi^{(bound)}_{J'} | \hat{\mathcal{O}}^\dagger_\lambda | \Phi^i_J \rangle \langle \Phi^i_J | \hat{\mathcal{O}}_\lambda | \Phi^{(bound)}_{J'} \rangle \delta(E - E_i), \tag{26}$$

where for simplicity we have suppressed the indices referring to the projections of the angular momenta, the summation i runs over all the discrete states whose wave function is given by Φ^i_J (the continuum states among them), and where $\Phi^{(bound)}_{J'}$ is the wave function of the bound state.

In appendix C we have summarized the Green's function formalism used in [4], which permits to relate the transition strength Eq.(26) to the imaginary part of the so called response function given by Eq. (63). This connection is given by Eq.(65), which for the case of discrete continuum states takes the form:

$$\frac{d\mathcal{B}^{(\lambda)}}{dE}(J' \to J) = -\frac{1}{\pi} Im \left[\sum_i \frac{\langle \Phi^{(bound)}_{J'} | \hat{\mathcal{O}}^\dagger_\lambda | \Phi^i_J \rangle \langle \Phi^i_J | \hat{\mathcal{O}}_\lambda | \Phi^{(bound)}_{J'} \rangle}{E - E_i} \right]. \tag{27}$$

The calculation of Eq.(27) is particularly simple when performing a complex scaling transformation, in such a way that the wave functions, the operator, and the eigenvalues in Eq.(27) become complex quantities. In fact, after complex scaling the discrete complex scaled states, for instance the ones shown in Fig.4, still form a complete basis [25]. The advantage of this method is that all the E_i-values are now complex and the initial energy E is still real. This means that the summation in Eq.(27) can now be easily made for all values of $E > 0$ (only the energies of the bound states, if any, are still real, but negative).

Therefore, after complex scaling of the $\alpha - \alpha$ potential, and imposing a box boundary condition, one gets the family of discrete eigenvalues shown in Fig.4, each of them associated to a complex rotated wave function. These functions are the complex rotated version of Eqs.(45) and (46). Using also the complex scaled version of the electromagnetic operator Eq.(44) one can compute the matrix elements in Eq.(27) and thereby the transition strength and the cross section.

In the case of transitions from continuum to continuum the response function Eq.(63) has to be written as:

$$\mathcal{R}_\lambda(E, E') = \sum_j \frac{1}{E' - E'_j} \sum_i \frac{\langle \Phi^{(j)}_{J'}(E'_j) | \hat{\mathcal{O}}^\dagger_\lambda | \Phi^i_J(E_i) \rangle \langle \Phi^i_J(E_i) | \hat{\mathcal{O}}_\lambda | \Phi^{(j)}_{J'}(E'_j) \rangle}{E - E_i}, \tag{28}$$

where i and j run over the initial and final (discrete) continuum spectrum, where we have written explicitly the dependence of each wave function on the (complex) discrete energies E_i and E'_j, and where E and E' are the (real) initial and final energies.

Making use now twice of Eq.(64) we get the analogous to Eq.(27) for continuum to continuum transitions:

$$\begin{aligned}
&\mathcal{R}_\lambda(E,E') = \\
&P.V.\left[\sum_j \frac{1}{E'-E'_j} P.V.\left[\sum_i \frac{\langle \Phi^{(j)}_{J'}(E'_j)|\hat{\mathcal{O}}^\dagger_\lambda|\Phi^i_J(E_i)\rangle\langle\Phi^i_J(E_i)|\hat{\mathcal{O}}_\lambda|\Phi^{(j)}_{J'}(E'_j)\rangle}{E-E_i}\right]\right] - \\
&-\pi^2 \sum_{ij} \langle \Phi^{(j)}_{J'}(E'_j)|\hat{\mathcal{O}}^\dagger_\lambda|\Phi^i_J(E_i)\rangle\langle\Phi^i_J(E_i)|\hat{\mathcal{O}}_\lambda|\Phi^{(j)}_{J'}(E'_j)\rangle \delta(E-E_i)\delta(E'-E'_j) \qquad (29)\\
&-i\pi P.V.\left[\sum_j \frac{\sum_i \langle \Phi^{(j)}_{J'}(E'_j)|\hat{\mathcal{O}}^\dagger_\lambda|\Phi^i_J(E_i)\rangle\langle\Phi^i_J(E_i)|\hat{\mathcal{O}}_\lambda|\Phi^{(j)}_{J'}(E'_j)\rangle \delta(E-E_i)}{E'-E'_j}\right] \\
&-i\pi \sum_j P.V.\left[\sum_i \frac{\langle \Phi^{(j)}_{J'}(E'_j)|\hat{\mathcal{O}}^\dagger_\lambda|\Phi^i_J(E_i)\rangle\langle\Phi^i_J(E_i)|\hat{\mathcal{O}}_\lambda|\Phi^{(j)}_{J'}(E'_j)\rangle}{E-E_i}\right]\delta(E'-E'_j),
\end{aligned}$$

where *P.V.* means the Principal Value of the corresponding integral.

As we can see from the expression above, the transition strength Eq.(40) is contained in the real part of the response function Eq.(28). Unfortunately, this real part is contaminated by a double Principal Value, which is also real. Use of a complex scaling transformation permits an easy calculation of the response function Eq.(28), and in particular of its real part. However, to eliminate from it the double principal value given in Eq.(29) can be a rather complicated task. For this reason, the use of the complex scaling method to compute bremsstrahlung cross sections appears to be complicate. The exception can be those cases where a very well defined and narrow resonance is present in the final state. This happens for instance in the $2^+ \to 0^+$ transition in ^{8}Be, where the very low-lying 0^+ resonance is so narrow that it can be treated as a bound state, and therefore Eq.(27) can still be used.

4.2 Complex scaling: $E2$-capture in the $2^+ \to 0^+$ transition in ^{8}Be.

We shall start this section by making the s-wave α-α interaction (in principle described by the Buck potential [11]) slightly more attractive, such that the low-lying 0^+ resonance becomes a true bound state. Under these conditions, after a complex scaling calculation of the initial and final states, Eq.(27) can be used safely. With the radial matrix elements computed in this way, the cross section is then obtained from Eq.(1), where $E_\gamma = E - E_B$, with E_B being the binding energy of the artificially bound 0^+ state.

The dashed line in Fig.5 shows the computed cross section when the 0^+ state has a binding energy of $E_B = -25$ keV. The calculation has been done with a complex scaling angle $\theta = 0.25$ rads., but the result is of course independent of the angle used. For comparison, we also show in the figure the cross section given in Fig.2a (dotted curve), corresponding to a calculation on the real energy axis with the true Buck potential. As we can see, the increase in the 0^+ binding energy produces an increase in the cross section, with a maximum value that goes up from about 14 nb to about 19 nb. In fact, for a smaller binding like $E_B = -3$ keV (dot-dashed curve in the figure) the maximum of the cross section goes down to 18 nb.

If we still reduce the attraction in the s-wave α-α potential the bound 0^+ state becomes a true resonance. Still using Eq.(27), we then get the cross sections shown by the dot-dot-dashed curve, which corresponds to a 0^+ resonance energy of 34 keV, and the dashed-dashed-dot curve, which corresponds to a 0^+ resonance energy of 57 keV. As we can see, the more the resonance energy approaches the experimental value of 92 keV, the more the cross section approaches the result obtained on the real energy axis. However, for a resonance energy of 57 keV, we observe that at some point, in the vicinity of $E = 4$ MeV, the cross section is negative, which is already an indication that use of Eq.(27) is not fully correct for all energies. First, the energy of the final state is not fully real, and the square of the radial matrix element Eq.(15) would be in general complex. Therefore it can not be the real quantity given by Eq.(27). And second, the contributions not included in the calculation (transitions to the continuum 0^+ states) have already some role to play. In fact, when the correct Buck potential is used for the s-wave interaction (0^+ resonance at 92 keV), the cross section obtained from Eq.(27),

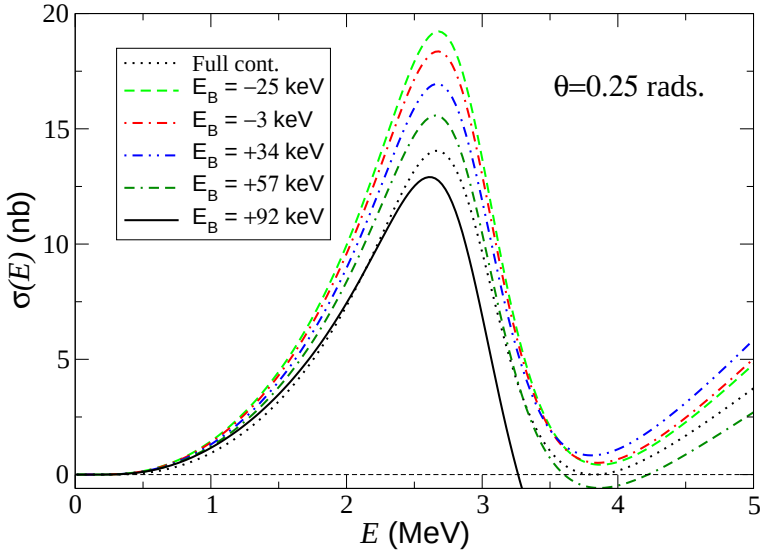

Fig. 5 Cross section for the $2^+ \rightarrow 0^+$ transition into the ground state of ^{8}Be for different energies (E_B) of the 0^+ state. The complex scaling calculation has been made with a complex scaling angle of 0.25 rads. The result given in Fig.2a (dotted curve) is shown for comparison.

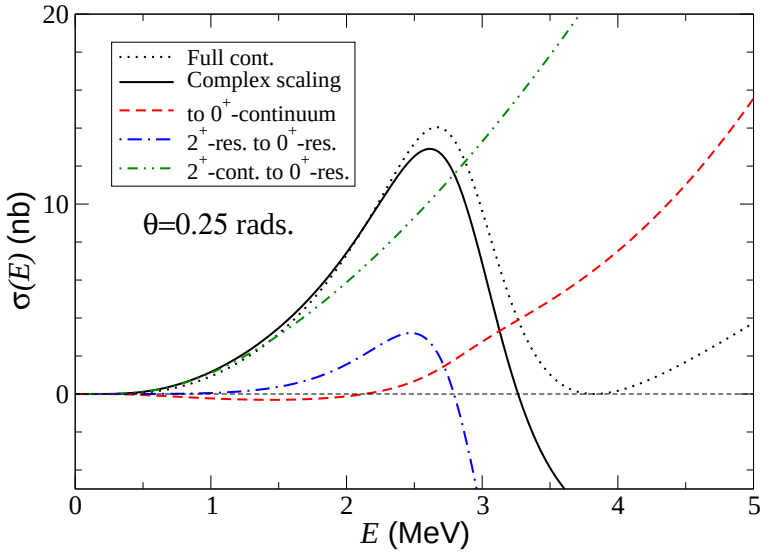

Fig. 6 Contributions of the different transitions to the bremsstrahlung cross section for the $2^+ \rightarrow 0^+$ transition in ^{8}Be. The scaling angle θ has been taken equal to 0.25 rads. The solid line gives the total cross section obtained from Eq.(27) assuming transitions to the 0^+ resonance only (which is treated as a bound state). The dotted line is the cross section obtained with a full continuum calculation on the real energy axis (Fig.2a). The difference between these two curves is given by the dashed curve. The contributions from the resonance-resonance and continuum-resonance transitions given by Eq.(27) are shown by the dot-dashed and the dot-dot-dashed curves, respectively.

solid curve in the figure, becomes very negative for initial energies higher than about 3 MeV. Also, the maximum of the cross section is 1.5 nb below the result shown in Fig.2a.

In any case, even if Eq.(27) does not contain the full information about the cross section, it can be used to extract some of the contributions to it. In particular, the summation in the r.h.s. of the equation permits to separate the contribution of transitions from the continuum 2^+ states to the resonant 0^+ state (continuum-resonance contribution), and the contribution corresponding to a resonance-resonance transition. Of course, for this separation to be possible, a complex scaling angle larger than the argu-

ment of the 2^+ resonance is required. This is already indicating that this separation between different types of contributions depends on the complex scaling angle.

The different contributions are shown in Fig.6, where we plot again the solid and dotted curves already shown in Fig.5, which correspond to the cross section obtained from Eq.(27) assuming transitions to the 0^+ resonance only (and treated as a bound state), and the full cross section computed on the real energy axis. The difference between these two curves (dashed curve in the figure) represents the effect of, first, the transitions to continuum 0^+ states not included in Eq.(27), and, second, the fact that Eq.(27) is not really valid for unbound final states (Eq.(29) should be used instead). Due to very small width of the 0^+ resonance, the effect shown by the dashed curve in Fig.6 is expected to come mainly from the missing transitions to the continuum 0^+ states. The resonance-resonance and continuum-resonance contributions obtained from Eq.(27) are shown by the dot-dashed and dot-dot-dashed curves, respectively. As we can see, the resonance-resonance contribution shows a peak at about the 2^+ resonance energy, but right after the peak goes sharply down and it actually becomes very negative. This very negative contribution has to be compensated by the remaining ones, especially by the continuum-resonance contribution. However, even this is not enough, and the transitions to continuum final states play an important role.

5 Summary and conclusions

In this work we have revisited the problem of bremsstrahlung radiation in two-body collisions, which is equivalent to a gamma decay process between continuum states. The case of the $E2$ transitions in α+α collisions is taken as an example, and used to test the methods.

We have given the details, related, and compared three different procedures. In two of them the energies of the initial and final states are kept on the real energy axis. The main difference between them is in the way how the continuum states are treated. In the first method they are obtained with the correct asymptotic behavior, which implies an orthogonality between states in the continuum sense, with a Dirac delta. In the second method the continuum is discretized by imposing a box boundary condition. The continuum states are zero outside the box, and they are treated as bound states, and therefore normalized to 1 inside the box. Both procedures are of course consistent, and they have been shown to be fully equivalent in the limit of an infinitely big box. However, when very narrow resonances are involved in the reaction under investigation, a correct description of such resonance with the second method requires a huge discretization box, making this second procedure impractical for these cases (like the $2^+ \to 0^+$ process in ^{8}Be). Although formally it is not needed, the numerical implementation of these two methods is very much simplified after regularization of the radial integrals involved in the calculation. In this work the Zel'dovich prescription has been used.

The third procedure is based on the complex scaling method. After complex scaling the resonances appear formally as bound states with complex energy, and they are then well identified and differentiated from ordinary continuum states. Once this is done, it is then, at least in principle, possible to separate the contribution from the different types of transition, namely, from resonance to resonance, from continuum states to resonance, from resonance to continuum, and from continuum to continuum. However, although the method works well for transitions into bound states, we have shown that when the final state is unbound the extraction of the radial integrals requires knowledge of a double Principal Value, which makes the whole procedure not easy to implement. For sufficiently low-lying narrow resonances in the final state the complex scaling procedure still provides a rather good approximation of the bremsstrahlung radiation cross section, making possible to estimate the different contributions. In any case, even if the separation into different contributions is made, only the sum of all of them is an observable physics quantity.

Acknowledgements This work was partly supported by funds provided by DGI of MINECO (Spain) under contract No. FIS2011-23565.

A Energy normalization of the continuum wave functions

Let us start with a partial wave expansion of a two-body wave function:

$$\Psi(\boldsymbol{k},\boldsymbol{r}) = \frac{1}{C}\sqrt{\frac{2}{\pi}}\frac{1}{kr}\sum_{\ell} i^{\ell} u_{\ell}(k,r)\sum_{m} Y_{\ell m}(\Omega_r)Y^{*}_{\ell m}(\Omega_k). \tag{30}$$

In the expression above the constant C can in principle be anything. The only requirement is that the radial wave functions u_ℓ have to be normalized in such a way that Ψ reduces to a plane wave in the limit of no interaction between particles. In other words, Ψ has to fulfill that:

$$\begin{aligned}\Psi(\boldsymbol{k},\boldsymbol{r}) &\overset{\text{free case}}{\rightarrow} \frac{1}{(2\pi)^{3/2}} e^{i\boldsymbol{k}\cdot\boldsymbol{r}} \\ &= \sqrt{\frac{2}{\pi}}\sum_{\ell} i^{\ell} j_{\ell}(kr)\sum_{m} Y_{\ell m}(\Omega_r)Y^{*}_{\ell m}(\Omega_k),\end{aligned} \tag{31}$$

from where it is obvious that u_ℓ must satisfy:

$$u_{\ell}(k,r) \overset{\text{free case}}{\rightarrow} Ckrj_{\ell}(kr). \tag{32}$$

If we now make use of the fact that:

$$\int_0^{\infty} krj_{\ell}(kr)k'rj_{\ell}(k'r)dr = \frac{\pi}{2}\delta(k-k'), \tag{33}$$

we then immediately see that the radial wave functions u_ℓ satisfy the normalization condition:

$$\int_0^{\infty} u_{\ell}(k,r)u_{\ell}(k',r)dr = C^2\frac{\pi}{2}\delta(k-k'). \tag{34}$$

Therefore, if we choose $C=\sqrt{2/\pi}$ the radial wave functions would satisfy the so-called momentum normalization.

Since $k=\sqrt{2\mu E/\hbar^2}$, it is not difficult to see that:

$$\delta(k-k') = \delta(\sqrt{\frac{2\mu E}{\hbar^2}} - \sqrt{\frac{2\mu E'}{\hbar^2}}) = \frac{\hbar^2 k}{\mu}\delta(E-E'), \tag{35}$$

which leads to:

$$\int_0^{\infty} u_{\ell}(k,r)u_{\ell}(k',r)dr = C^2\frac{\pi}{2}\frac{\hbar^2 k}{\mu}\delta(E-E'), \tag{36}$$

which implies that, as given in Eq.(5), by choosing

$$C = \sqrt{\frac{2\mu}{\pi\hbar^2 k}} \tag{37}$$

the energy normalization condition

$$\int_0^{\infty} u_{\ell}(k,r)u_{\ell}(k',r)dr = \delta(E-E') \tag{38}$$

is then satisfied.

B Radiative capture cross section.

Let us consider the photodissociation reaction $A+\gamma \rightarrow a+b$, and let us denote by J' and J the angular momenta of the system A and the continuum two-body system ab, respectively. The corresponding photodissociation cross section (with multipolarity λ) can be found in Ref.[20] for the case in which A represents a bound state. When the state A corresponds also to a two-body continuum state (made of particles a and b) the expression in Ref.[20] can be generalized to:

$$\frac{d\sigma_{\gamma}^{(\lambda)}}{dE'}(E) = \frac{(2\pi)^3(\lambda+1)}{\lambda\left[(2\lambda+1)!!\right]^2}\left(\frac{E_\gamma}{\hbar c}\right)^{2\lambda-1}\frac{d\mathcal{B}^{(\lambda)}}{dEdE'}(J'\rightarrow J), \tag{39}$$

where E and E' are the energies of the final and initial states, and E_γ is the photon energy.

We shall assume the initial and final continuum spectra to be discretized, in such a way that the transition strength $d\mathcal{B}^{(\lambda)}/dEdE'$ can be written as [20]:

$$\frac{d\mathcal{B}^{(\lambda)}}{dEdE'}(J' \to J) = \frac{1}{2J'+1}\sum_{i,j}|\langle\Phi^i_J||\hat{O}_\lambda||\Phi^j_{J'}\rangle|^2\delta(E-E_i)\delta(E'-E'_j)$$
$$= \sum_{i,j}\sum_{m,\mu}|\langle\Phi^i_{J\mu}|\hat{O}_{\lambda m}|\Phi^j_{J'\mu'}\rangle|^2\delta(E-E_i)\delta(E'-E'_j), \quad (40)$$

where $|\Phi^j_{J'\mu'}\rangle$ and $|\Phi^i_{J\mu}\rangle$ are the wave functions describing the continuum state A (with energy E'_j and angular momentum and projection $J'\mu'$), and of the continuum final ab-system (with energy E_i and angular momentum and projection $J\mu$), respectively. The operator $\hat{O}_\lambda$ is the electromagnetic transition operator with rank λ, and the indices i and j run over all the (discrete) initial and final continuum states.

From this expression it is easy to connect the transition strength for a given reaction and the inverse one:

$$\frac{d\mathcal{B}^{(\lambda)}}{dEdE'}(J' \to J) = \frac{2J+1}{2J'+1}\frac{d\mathcal{B}^{(\lambda)}}{dEdE'}(J \to J'). \quad (41)$$

The photoabsorption cross section in Eq.(39) and the one corresponding to the inverse process, i.e., the radiative capture cross section $\sigma^{(\lambda)}(E)$ for the process $a+b \to A+\gamma$, are related by the detailed balance principle, which is given in Eq.(3) of [20]:

$$\frac{d\sigma^{(\lambda)}}{dE'}(E) = \frac{2(2J'+1)}{(2J_a+1)(2J_b+1)}\frac{1}{k^2}\left(\frac{E_\gamma}{\hbar c}\right)^2\frac{d\sigma^{(\lambda)}_\gamma}{dE'}(E), \quad (42)$$

where J_a and J_b are the angular momenta of particles a and b, respectively, and $k^2 = 2\mu_{ab}E/\hbar^2$. Thanks to this relation, and making use of Eqs.(39) and (41) we find the following general expression for the radiative capture cross section $a+b \to A+\gamma$:

$$\frac{d\sigma^{(\lambda)}}{dE'}(E) = \frac{(2\pi)^3(\lambda+1)}{\lambda\left[(2\lambda+1)!!\right]^2}\frac{1}{k^2}\frac{2(2J+1)}{(2J_a+1)(2J_b+1)}\left(\frac{E_\gamma}{\hbar c}\right)^{2\lambda+1}\frac{d\mathcal{B}^{(\lambda)}}{dEdE'}(J \to J'). \quad (43)$$

Let us consider now that particles a and b are identical, with spin zero, and with charge Ze (with e the electron charge). For the case of an electric transition process of order λ the electromagnetic transition operator reads:

$$\hat{O}_{\lambda m} = e\sum_{n=1}^{2} Z_n r_n^\lambda Y_{\lambda m}(\Omega_r) = \frac{Ze}{2^{\lambda-1}}r^\lambda Y_{\lambda m}(\Omega_r), \quad (44)$$

where $\boldsymbol{r} = \boldsymbol{r}_1 - \boldsymbol{r}_2$ and $\boldsymbol{r}_n$ is the center of mass coordinate of particle n.

Assuming now a central interaction between the two particles, the two-body wave functions involved in Eq.(40) can be written as:

$$\Phi^j_{J'\mu'}(\boldsymbol{r}) = \frac{u^{(j)}_{J'}(E'_j,r)}{r}Y_{J'\mu'}(\Omega_r) \quad (45)$$

$$\Phi^i_{J\mu}(\boldsymbol{r}) = \frac{u^{(i)}_{J}(E_i,r)}{r}Y_{J\mu}(\Omega_r), \quad (46)$$

Inserting the expressions above and Eq.(44) into Eq.(40), and after analytical integration over the angular coordinates, we get that:

$$\frac{d\mathcal{B}^{(\lambda)}}{dEdE'}(J \to J') = \frac{(Ze)^2}{2^{2\lambda-2}}\frac{1}{4\pi}\sum_{i,j}\delta(E-E_i)\delta(E'-E'_j)(2\lambda+1)\left|\langle J0;\lambda 0|J'0\rangle\int dr u^{(i)}_J(E_i,r)r^\lambda u^{(j)}_{J'}(E'_j,r)\right|^2, \quad (47)$$

from which Eq.(43), corresponding to the $E\lambda$ radiative capture process $a+b \to A+\gamma$, takes the final form:

$$\frac{d\sigma^{(\lambda)}}{dE'}(E) = \frac{(Ze)^2}{2^{2\lambda-2}}\frac{2\pi^2(\lambda+1)}{\lambda\left[(2\lambda+1)!!\right]^2}\frac{1}{k^2}\frac{2(2J+1)}{(2J_a+1)(2J_b+1)}$$
$$\times\sum_{i,j}\left(\frac{E_\gamma}{\hbar c}\right)^{2\lambda+1}\delta(E-E_i)\delta(E'-E'_j)(2\lambda+1)\left|\langle J0;\lambda 0|J'0\rangle\int dr u^{(i)}_J(E_i,r)r^\lambda u^{(j)}_{J'}(E'_j,r)\right|^2. \quad (48)$$

In the particular case of two α particles ($J_a = J_b = 0$, $Z = 2$) and an electric quadrupole transition ($\lambda = 2$), and after integration over E', we get for the total cross section:

$$\sigma^{(\lambda)}(E) = \frac{2\pi^2e^2}{15k^2}(2\ell+1)\langle\ell 0;20|\ell' 0\rangle^2\sum_{i,j}\left(\frac{E_\gamma}{\hbar c}\right)^5\delta(E-E_i)\left|\int dr u^{(i)}_\ell(E_i,r)r^2u^{(j)}_{\ell'}(E'_j,r)\right|^2, \quad (49)$$

where we have replaced J by ℓ and J' by ℓ'.

This result agrees with the one given in Eq.(24), which in turns comes from the general expression Eq.(1), except for a factor of 2. This difference comes from the factor of 2 introduced in [1; 8] due to the fact that we are dealing with two identical particles (see for instance Eq.(9) in Ref. [8]).

C Green's function formalism

In this section we summarize the aspects of the Green's function formalism that are relevant for this work. All the details can be found in [24].

Let us consider a system whose hamiltonian operator is given by $\hat{\mathcal{H}}$, and such that its spectrum is formed by a set of discrete states $\{|\Phi_n\rangle\}$ and the continuum states $|\Phi_c\rangle$. The eigenfunctions form a complete basis, and the unity operator takes the form:

$$\mathbb{1} = \sum_n |\Phi_n\rangle\langle\Phi_n| + \int dE_c |\Phi_c\rangle\langle\Phi_c|. \tag{50}$$

If $|\boldsymbol{r}\rangle$ denotes the eigenvector of the position operator, we have that $\langle\boldsymbol{r}|\boldsymbol{r}'\rangle = \delta(\boldsymbol{r}-\boldsymbol{r}')$, the unity operator can also be written as

$$\mathbb{1} = \int d\boldsymbol{r} |\boldsymbol{r}\rangle\langle\boldsymbol{r}|, \tag{51}$$

and the Schrödinger equation $\hat{\mathcal{H}}|\Phi_n\rangle = E_n|\Phi_n\rangle$ can be written in coordinate space as:

$$\int d\boldsymbol{r} d\boldsymbol{r}' |\boldsymbol{r}\rangle\langle\boldsymbol{r}|\hat{\mathcal{H}}|\boldsymbol{r}'\rangle\langle\boldsymbol{r}'|\Phi_n\rangle = \int d\boldsymbol{r} E_n |\boldsymbol{r}\rangle\langle\boldsymbol{r}|\Phi_n\rangle. \tag{52}$$

The functions $\langle\boldsymbol{r}|\Phi_n\rangle = \Phi_n(\boldsymbol{r})$ are the eigenfunctions of the hamiltonian in coordinate space, $\mathcal{H}(\boldsymbol{r})\Phi_n(\boldsymbol{r}) = E_n\Phi_n(\boldsymbol{r})$, is such a way the equation above can be written also as:

$$\int d\boldsymbol{r} d\boldsymbol{r}' |\boldsymbol{r}\rangle\langle\boldsymbol{r}|\hat{\mathcal{H}}|\boldsymbol{r}'\rangle\Phi_n(\boldsymbol{r}') = \int d\boldsymbol{r} |\boldsymbol{r}\rangle\mathcal{H}(\boldsymbol{r})\Phi_n(\boldsymbol{r}), \tag{53}$$

from which we can immediately get that:

$$\langle\boldsymbol{r}|\hat{\mathcal{H}}|\boldsymbol{r}'\rangle = \mathcal{H}(\boldsymbol{r})\delta(\boldsymbol{r}-\boldsymbol{r}'). \tag{54}$$

The Green's function for a given energy E is defined as the function $G(E;\boldsymbol{r},\boldsymbol{r}')$ satisfying that:

$$\left(E - \mathcal{H}(\boldsymbol{r})\right) G(E;\boldsymbol{r},\boldsymbol{r}') = \delta(\boldsymbol{r}-\boldsymbol{r}'). \tag{55}$$

The Green's function can also be defined in terms of the operator $\hat{G}(E)$, such that:

$$G(E;\boldsymbol{r},\boldsymbol{r}') = \langle\boldsymbol{r}|\hat{G}(E)|\boldsymbol{r}'\rangle. \tag{56}$$

The form of the $\hat{G}(E)$ operator can be obtained by noting that:

$$\langle\boldsymbol{r}|(E-\hat{\mathcal{H}})\hat{G}(E)|\boldsymbol{r}'\rangle = \int d\boldsymbol{r}'' \langle\boldsymbol{r}|E-\hat{\mathcal{H}}|\boldsymbol{r}''\rangle\langle\boldsymbol{r}''|\hat{G}(E)|\boldsymbol{r}'\rangle, \tag{57}$$

where we have made use of Eq.(51). Having now in mind Eqs.(54) and (56), the expression above then reads:

$$\langle\boldsymbol{r}|(E-\hat{\mathcal{H}})\hat{G}(E)|\boldsymbol{r}'\rangle = \int d\boldsymbol{r}'' \delta(\boldsymbol{r}-\boldsymbol{r}'')(E-\mathcal{H}(\boldsymbol{r}))G(E;\boldsymbol{r},\boldsymbol{r}'), \tag{58}$$

which due to Eq.(55) leads to:

$$\langle\boldsymbol{r}|(E-\hat{\mathcal{H}})\hat{G}(E)|\boldsymbol{r}'\rangle = \delta(\boldsymbol{r}-\boldsymbol{r}'), \tag{59}$$

or, in other words:

$$\hat{G}(E) = \frac{\mathbb{1}}{E-\hat{\mathcal{H}}}. \tag{60}$$

Application of the operator (60) on the unity operator (50) permits to write:

$$\hat{G}(E) = \sum_n \frac{|\Phi_n\rangle\langle\Phi_n|}{E-E_n} + \int dE_c \frac{|\Phi_c\rangle\langle\Phi_c|}{E-E_c}, \tag{61}$$

or, by the definition (56):

$$G(E;\boldsymbol{r},\boldsymbol{r}') = \sum_n \frac{\Phi_n(\boldsymbol{r})\Phi_n^*(\boldsymbol{r}')}{E-E_n} + \int dE_c \frac{\Phi_c(\boldsymbol{r})\Phi_c^*(\boldsymbol{r}')}{E-E_c}. \tag{62}$$

Let us consider now some operator $\hat{\mathcal{O}}$, and let us consider the matrix element $\langle\Phi_n|\hat{\mathcal{O}}^\dagger\hat{G}(E)\hat{\mathcal{O}}|\Phi_n\rangle$, which thanks to Eq.(61) can be written as:

$$\langle\Phi_n|\hat{\mathcal{O}}^\dagger\hat{G}(E)\hat{\mathcal{O}}|\Phi_n\rangle = \sum_m \frac{\langle\Phi_n|\hat{\mathcal{O}}^\dagger|\Phi_m\rangle\langle\Phi_m|\hat{\mathcal{O}}|\Phi_n\rangle}{E-E_m} + \int dE_c \frac{\langle\Phi_n|\hat{\mathcal{O}}^\dagger|\Phi_c\rangle\langle\Phi_c|\hat{\mathcal{O}}|\Phi_n\rangle}{E-E_c}. \tag{63}$$

If the hamiltonian $\hat{\mathcal{H}}$ is hermitian all the eigenvalues are real, and the function above has a series of poles on the real energy axis. The expression above has to be computed making use of:

$$\lim_{y\to 0^+}\int_A^B \frac{f(x)}{x\pm iy}dx = \\ \lim_{\alpha\to 0^+}\left[\int_A^{-\alpha}\frac{f(x)}{x}dx + \int_\alpha^B \frac{f(x)}{x}dx\right] \mp i\pi\int dx f(x)\delta(x) = P.V.\left[\int_A^B \frac{f(x)}{x}dx\right] \mp i\pi\int dx f(x)\delta(x), \tag{64}$$

where $A<0<B$ and $f(x)$ is a function well behaved in the interval $[A,B]$, and where *P.V.* refers to the Principal Value of the integral. Using (64) we can then obtain:

$$\sum_m \langle\Phi_n|\hat{\mathcal{O}}^\dagger|\Phi_m\rangle\langle\Phi_m|\hat{\mathcal{O}}|\Phi_n\rangle\delta(E-E_m) + \int dE_c\langle\Phi_n|\hat{\mathcal{O}}^\dagger|\Phi_c\rangle\langle\Phi_c|\hat{\mathcal{O}}|\Phi_n\rangle\delta(E-E_c) = -\frac{1}{\pi}Im\left(\langle\Phi_n|\hat{\mathcal{O}}^\dagger\hat{G}(E)\hat{\mathcal{O}}|\Phi_n\rangle\right). \tag{65}$$

The function $\langle\Phi_n|\hat{\mathcal{O}}^\dagger\hat{G}(E)\hat{\mathcal{O}}|\Phi_n\rangle$ is what, for instance in Ref.[4], is called the response function, from which the strength function can be extracted according to Eq.(65).

References

1. K. Alder, A. Bohr, T. Huus, B. Mottelson, and A. Winther, Rev. Mod. Phys. **28** (1956) 432.
2. K. Langanke and C. Rolfs, Phys. Rev. C **33** (1986) 790.
3. C.A. Bertulani, D.T. de Paula, and V.G. Zelevinsky, Phys. Rev. C **60** (1999) 031602.
4. T. Myo, A. Ohnioshi, and K. Kato, Prog. Theor. Phys. **99** (1998) 801.
5. Y.K. Ho, Phys. Rep. **99** (1983) 1.
6. E. Garrido, A.S. Jensen, and D.V. Fedorov, Phys. Rev. C **86** (2013) 064608.
7. E. Garrido, A.S. Jensen, and D.V. Fedorov, submitted for publication.
8. O. Tanimura and U. Mosel, Nucl. Phys. A **440** (1985) 173.
9. Ya.B. Zel'dovich, Zh. Exp. Theor. Fiz. **39** (1960) 776.
10. K. Langanke, Phys. Lett. B **174** (1986) 27.
11. B. Buck, H. Friedrich, and C. Wheatley, Nucl. Phys. A **275** (1977) 246.
12. S. Ali and A.R. Bodmer, Nucl. Phys. A **80** (1966) 99.
13. D. Krolle, H.J. Assenbaum, C. Funk, and K. Langanke, Phys. Rev. C **35** (1987) 1631.
14. D.R. Tilley, J.H. Kelley, J.L. Godwin, D.J. Millener, J. Purcell, C.G. Sheu, and H.R. Weller, Nucl. Phys. A **745** (2004) 155.
15. K. Langanke and C. Rolfs, Z. Phys. A **324** (1986) 307.
16. W. Greiner, *Quantum Mechanics: Special chapters*, Springer-Verlag (2001) pp 121.
17. P. Mohr, H. Abele, V. Kölle, G. Staudt, H. Oberhummer, and H. Krauss, Z. Phys. A **349** (1994) 339.
18. C.A. Bertulani, Z. Phys. A **356** (1996) 293.
19. F.M. Nunes and I.J. Thompson, Phys. Rev. C **59** (1999) 2652.
20. C. Forssén, N.B. Shulgina, and M.V. Zhukov, Phys. Rev. C **67** (2003) 045801.
21. O.E. Alon and N. Moiseyev, Phys. Rev. A **46** (1992) 3807.
22. N. Moiseyev, Phys. Rep. **302** (1998) 247.
23. K. Kato, J. of Phys.: Conference Series **49** (2006) 73.
24. E.N. Economou, *Green's functions in quantum physics*, Springer Series in Solid-State Sciences 7, Springer-Verlag, Berlin-Heidelberg-New York (2006) Chapter 1.
25. B. Giraud and K. Kato, Ann. of Phys. **308** (2003) 115.